The alternative of CubeSat-based advanced infrared and microwave sounders for high impact weather forecasting

Zhenglong LI, Jun LI, Timothy J. SCHMIT, Pei WANG, Agnes LIM, Jinlong LI, Fredrick W. NAGLE, Wenguang BAI, Jason A. OTKIN, Robert ATLAS, Ross N. HOFFMAN, Sid-Ahmed BOUKABARA, Tong ZHU, William J. BLACKWELL & Thomas S. PAGANO

Taylor & Francis
Taylor & Francis Group

The alternative of CubeSat-based advanced infrared and microwave sounders for high impact weather forecasting

LI Zhenglong [ID]a, LI Juna, SCHMIT Timothy J.b, WANG Peia, LIM Agnesa, LI Jinlonga, NAGLE Fredrick W.a, BAI Wenguangc, OTKIN Jason A.a, ATLAS Robert [ID]d, HOFFMAN Ross N.d,e, BOUKABARA Sid-Ahmedf, ZHU Tongf,g, BLACKWELL William J.h and PAGANO Thomas S.i

aCooperative Institute for Meteorological Satellite Studies, University of Wisconsin-Madison, Madison, WI, USA; bCenter for Satellite Applications and Research, National Oceanic and Atmospheric Administration, Madison, WI, USA; cNational Satellite Meteorological Center, China Meteorological Administration, Beijing, China; dAtlantic Oceanographic and Meteorological Laboratory, Ocean and Atmospheric Research/ National Oceanic and Atmospheric Administration, Miami, FL, USA; eCooperative Institute for Marine and Atmospheric Studies, University of Miami, Miami, FL, USA; fCenter for Satellite Applications and Research, National Oceanic and Atmospheric Administration, College Park, MD, USA; gCooperative Institute for Research in the Atmosphere, Colorado State University, Fort Collins, CO, USA; hLincoln Laboratory, Massachusetts Institute of Technology, Lexington, MA, USA; iJet Propulsion Laboratory, California Institute of Technology, Pasadena, CA, USA

ABSTRACT

The advanced infrared (IR) and microwave (MW) sounding systems have been providing atmospheric sounding information critical for nowcasting and improving weather forecasts through data assimilation in numerical weather prediction. In recent years, advanced IR and MW sounder systems are being proposed to be onboard CubeSats that are much more cost efficient than traditional satellite systems. An impact study using a regional Observing System Simulation Experiment on a local severe storm (LSS) was carried out to evaluate the alternative of using advanced MW and IR sounders for high-impact weather forecasting in mitigating the potential data gap of the Advanced Technology Microwave Sounder (ATMS) and the Cross-track Infrared Sounder (CrIS) on the Suomi-NPP (SNPP) or Joint Polar Satellite System (JPSS). It was found that either MicroMAS-2 or the CubeSat Infrared Atmospheric Sounder (CIRAS) on a single CubeSat was able to provide a positive impact on the LSS forecast, and more CubeSats with increased data coverage yielded larger positive impacts. MicroMAS-2 has the potential to mitigate the loss of ATMS, and CIRAS the loss of CrIS, on SNPP or JPSS, especially when multiple CubeSats are launched. There are several approximations and limitations to the present study, but these represent efficiencies appropriate to the principal goal of the study — gauging the relative values of these sensors.

摘要

近年来，小卫星技术的发展给传统气象卫星提供了经济有效的替补方案。本文针对可能出现的传统气象卫星的缺失情形，借助快速的区域观测系统模拟试验，探索了利用小卫星填补空缺的可能性。研究表明，单个小卫星，无论是近红外高光谱还是微波探测仪，都能够对局地强风暴天气的预报有所改进。然而，为了填补传统卫星缺失带来的影响，需要发射三颗甚至更多的小卫星来增加观测的覆盖面，以弥补小卫星精度略低、通道略少的缺陷。

1. Introduction

Advanced infrared (IR) sounders (Menzel et al. 2018), such as the Atmospheric InfraRed Sounder (AIRS), the Infrared Atmospheric Sounding Interferometer (IASI), and the Cross-track Infrared Sounder (CrIS), along with the advanced microwave (MW) sounders, such as the Advanced Microwave Sounding Unit (AMSU) and the Advanced Technology Microwave Sounder (ATMS), play critical roles in improving numerical weather prediction (NWP) through data assimilation, and nowcasting (Li et al. 2011, 2012). Those traditional advanced IR and MW sounders, usually onboard polar-

orbit satellites with dimensions on the order of meters (i.e. 1.3 m × 1.3 m × 4.2 m for Suomi NPP (SNPP)), are expensive to build and launch due to the complexity of the system. For example, the total cost for SNPP and the Joint Polar Satellite System (JPSS) is estimated to be US$ 18.9 billion. In recent years, much more cost-efficient (with costs measured in millions, not billions of USD) IR and MW sounders have been proposed to be launched onboard 3U and 6U CubeSats, where 1U is defined as a 10 cm × 10 cm × 10 cm volume. Enabling technologies have been developed and are

Table 1. MicroMAS-2 spectral characteristics.

Band type	Channel	Center Frequency (GHz)	Bandwidth (GHz)
W-band	1	91.655 ± 2	1.000
F-band	2	114.50	1.000
	3	115.95	0.800
	4	116.65	0.600
	5	117.25	0.600
	6	117.80	0.500
	7	118.24	0.380
	8	118.58	0.300
G-band	9	183.31 ± 1.0	0.500
	10	183.31 ± 3.0	1.000
	11	183.31 ± 7.0	2.000
	12	204.30	3.000

being demonstrated for weather forecasting purposes. Two of these proposed satellites are the subject of this study.

First, Massachusetts Institute of Technology/Lincoln Laboratory (MIT/LL) followed up on its Micro-sized Microwave Atmospheric Satellite-1 (MicroMAS-1) experience with MicroMAS-2. While similar in design to MicroMAS-1 (e.g. 3U CubeSat), MicroMAS-2 has more channels (total of 12 channels: two imagery channels near 90 and 206 GHz; seven temperature channels near 118 GHz; and three moisture channels near 183 GHz (see Table 1 for details)), made possible by an additional miniaturized receiver, to provide more accurate temperature and moisture information. MicroMAS-2 also contains a slightly larger solar array in order to generate approximately 3 W of power for the payload, or about 60% more power than MicroMAS-1 (https://directory.eoportal.org/web/eoportal/satellite-missions/content/-/article/micromas-2).

Second, from its polar sun-synchronous orbit, the 6U CubeSat Infrared Atmospheric Sounder (CIRAS), an AIRS-like hyperspectral IR sounder, will measure the upwelling IR radiation of the Earth and its atmosphere in 625 shortwave IR (SWIR) spectral channels (1949–2451 cm^{-1}, or 4.08–5.13 μm, including the 4.3 μm CO_2 absorption band) (Pagano et al. 2017). CIRAS has a spectral resolution of 1.2–2.0 cm^{-1} and a Noise Equivalent differential Temperature (NEdT) of 0.1–0.4 K (increasing with frequency) at 250 K. The CIRAS horizontal resolution of 13.5 km covers a swath 1100 km wide. The observed radiances have information of potential value to operational forecast centers and can be used to derive lower tropospheric temperature and water vapor globally, as well as three-dimensional atmospheric motion vector winds (AMVs) for weather and climate science investigations. Multiple units would improve temporal coverage. CIRAS is scheduled for launch in the 2019 timeframe (https://www.jpl.nasa.gov/cubesat/missions/ciras.php).

The MicroMAS-2 and CIRAS sensors were both designed for use on CubeSats. CubeSat-based sounders usually have fewer spectral channels and a shorter

lifetime than traditional ones. They may be used to temporarily mitigate the data gap of traditional sounders. For example, if one or more sensors on NOAA's latest generation of polar orbiting satellites, the JPSS, are not available for some reason, CubeSats might be used to fill the data gap for the afternoon orbit. Thus, this study will address two questions: (1) Can the CubeSat-based advanced IR sounder and MW sounder be used to mitigate the loss of the current advanced sounders onboard the polar-orbit satellite systems? (2) What is the value of multiple CubeSats with such advanced sounders for local severe storm (LSS) forecasts? A regional observing system simulation experiment (OSSE) has been carried out to address the above two questions. This quick regional OSSE (R-OSSE) system has been used to study the value-added impact of geostationary advanced IR sounders, such as GIIRS (Geosynchronous Interferometric Infrared Sounder) onboard FengYun-4A (Yang et al. 2017), on high-impact weather forecasts (Li et al. 2018). The same procedure and case are used here for CubeSat sounder studies.

The rest of this paper is organized as follows: section 2 describes the simulation of CubeSat-based IR and MW advanced sounder observations; section 3 explains the assimilation strategies, experimental design, and evaluation procedure; section 4 reports the results of the impact studies; and section 5 provides a summary and discussion.

2. Cubesat-based MW and IR sounder system simulation

2.1. Orbit simulator

An orbit simulator was developed to simulate orbit tracks for a low earth satellite orbit. Li et al. (2018) used the orbit simulator to simulate orbits for existing satellites. The same orbit simulator was used in this study. Figure 1(a) shows the simulated satellite altitude and horizontal coverage for CIRAS and MicroMAS-2 in two different orbits – a polar orbit for CIRAS and a low (30°) inclination angle orbit for MicroMAS-2. Tables 1 and 2 list selected instrument parameters for MicroMAS-2 and CIRAS. Figure 1(b,c) show the temperature weighting functions for CIRAS and MicroMAS-2 using the US standard atmosphere 1976. Note that CIRAS has many more channels peaking in the troposphere, which should allow for a higher resolution description in the vertical direction of the troposphere, while MicroMAS-2 has channels that are sensitive to the upper troposphere and stratosphere, which should allow for a more complete description in the vertical direction. For each sensor, three polar orbits with different local equator crossing times were generated: 1030, 1330, and 1630 local time. The 1330 orbit
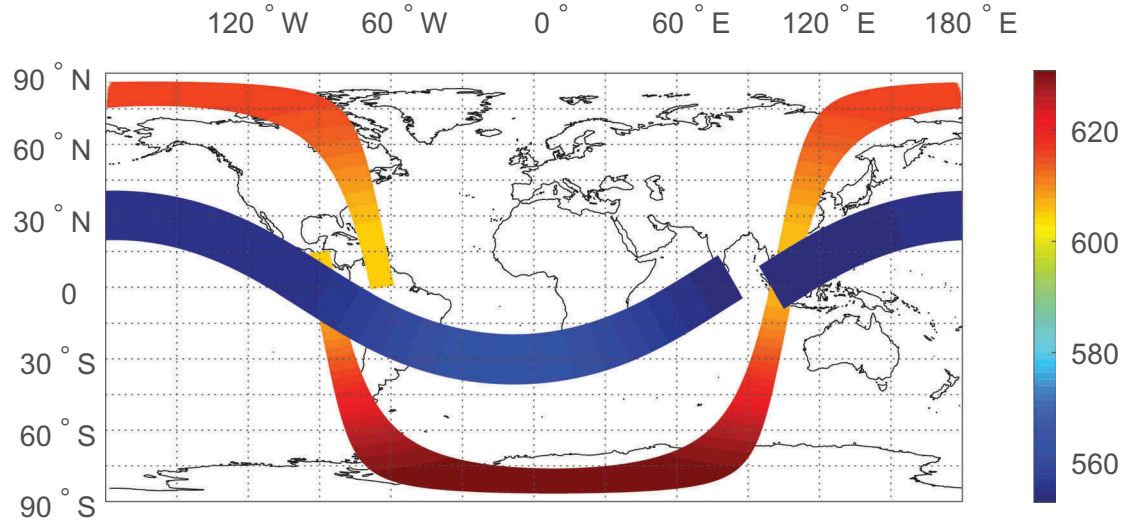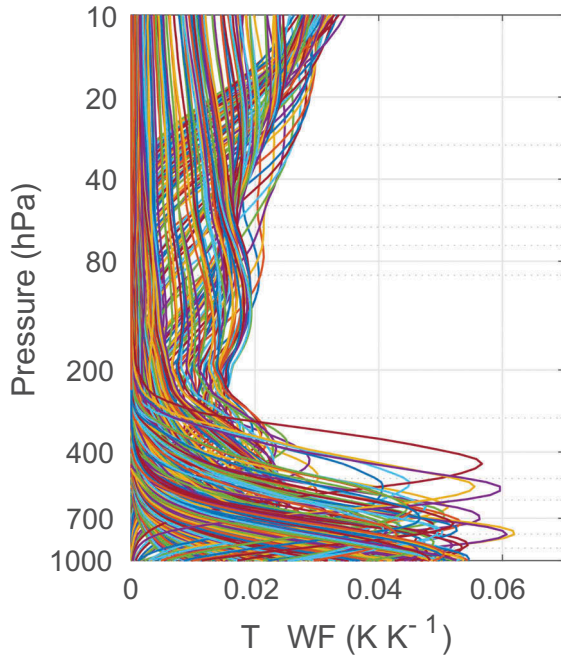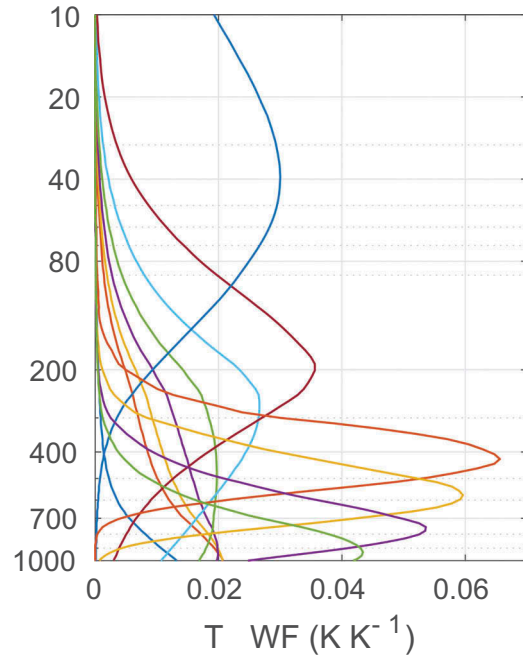
(a) Satellite altitude (km)

(b) CIRAS   (c) MicroMAS-2

Figure 1. (a) Simulated satellite altitude (units: km) and horizontal coverage of MicroMAS-2 and CIRAS, and (b, c) temperature weighting functions of (b) CIRAS and (c) MicroMAS-2 using the US standard atmosphere 1976. CIRAS is in the polar orbit (red to orange tones) and MicroMAS-2 is in the tropics orbit (inclination angle of 30°; blue tones).

matches that of SNPP and future JPSS satellites. The 1030 and 1630 orbits are included to increase the data coverage.

Table 2. Selected instrument parameters for CIRAS and MicorMAS-2.

	Altitude (km)	Scan angle (°)	Number of fields of view per scan line	Spatial resolution (km)
MicroMAS-2	550	± 60	81	15–30
CIRAS	600	± 42	64	13.5

2.2. Nature run

The same high-resolution nature run (HRNR) used by Li et al. (2018) was used in this study. A brief description is provided below. An LSS case is generated using WRF-NMM v3.6.1 with a spatial resolution of 2 km and 51 vertical layers from the surface to the 10-hPa model top. The HRNR covers almost the whole the continental United States and part of the eastern Pacific Ocean with a grid of 3200 × 1320 points (see Figure 2(a) for the
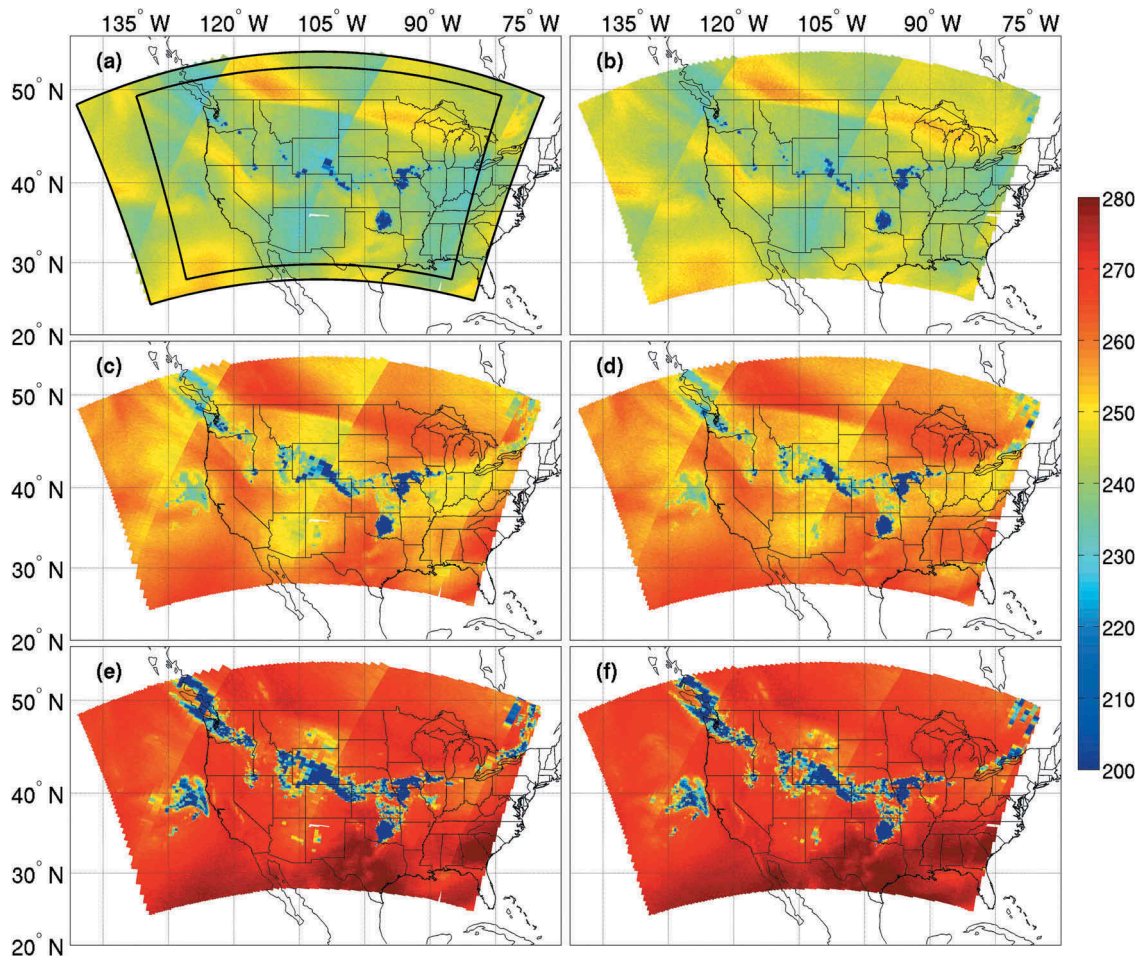
Figure 2. Simulated microwave brightness temperature (color bar; units: K) maps for MicroMAS-2 (left-hand column) and ATMS (right-hand column), for 0000–1200 UTC 27 May 2006, in the 183.31 ± 1.0 GHz (top row), 183.31 ± 3.0 GHz (middle row), and 183.31 ± 7.0 GHz (bottom row) channels. The two black frames in (a) denote the domains for the HRNR (outer frame) and for the data assimilation and forecast system (inner frame).

domain coverage). The HRNR is initialized at 1800 UTC 25 May 2006 from the global OSSE six-hourly analysis described by Lim et al. (2017), which also provides the boundary conditions. The HRNR evolves for 54 h until 0000 UTC 28 May 2006. The storm develops at 0000 UTC 27 May and lasts for 12 h. For a more detailed description of the HRNR, refer to Li et al. (2018).

2.3. Synthetic observation simulation

A simulator of synthetic satellite radiances was developed by combining the orbit simulator, an observation forward model, and the HRNR. First, the simulator linearly interpolates the HRNR variables needed for radiance simulation to the satellite observation times. All 2-km HRNR grid cells falling into the field of view (FOV) of CIRAS or MicroMAS-2 are averaged to generate the mean temperature, water vapor, and cloud hydrometer profiles. The forward model used is the

Community Radiative Transfer Model (CRTM; Chen et al. 2010; Chen, Han, and Weng 2012). Simulated observation errors are added as normal uncorrelated random numbers generated from instruments' specifications. CRTM has been widely used in simulating synthetic observations (Boukabara et al. 2018). The CRTM team (Tong Zhu and Sid Boukabara, personal communication, 2017) have developed and delivered the optical depth in pressure space coefficients required to use CRTM for both CIRAS and MicroMAS-2 based on the spectral response function (SRF) provided by JPL (Pagano et al. 2017) and MIT/LL (Blackwell et al. 2018). CRTM does not include nonlocal thermodynamic equilibrium (NLTE) effects in radiance simulation around the 4.3 μm CO_2 absorption band, which may contribute brightness temperature (T_b) error of about 1–1.5 K for those CIRAS channels. Ideally, NLTE effects should be included in the simulation of observations and in the assimilation of those

observations. However, in this study, we ignore NLTE effects both in the simulation and assimilation of the observations. This is equivalent to assuming a perfect simulation of NLTE effects in CRTM.

None of the existing MW sounders has the exact same 12 spectral channels as MicroMAS-2. However, MicroMAS-2 and ATMS have three similar moisture channels. Figure 2 compares the simulated T_b for these instruments for these three channels from 0000 to 1200 UTC 27 May 2006. Despite various differences in simulation, including satellite altitude, FOVs, SRFs, the three channels show very similar patterns for MicroMAS-2 and ATMS. Note the low T_b values in Oklahoma, Missouri, and Iowa denote the locations of the LSS at the time of the satellite overpass around 0825 UTC. Figure 3 shows the density scatterplots of the three channels in clear sky for the same time period. The relatively small bias (ATMS minus MicroMAS-2), small standard deviation (STD), and large correlation coefficients, indicate that the three channels on the two instruments are similar. Note that the 183.31 ± 7.0 GHz channel has the fewest clear-sky observations because it peaks lowest among the three channels.

Comparison between CIRAS and CrIS/IASI shows excellent agreement for one randomly chosen atmospheric profile Figure 4. In Figure 4, the left-hand side is the H_2O band used for humidity sounding and the right-hand side is the CO_2 band used for temperature sounding. Since CIRAS has a spectral resolution of 1.2–2.0 cm^{-1}, coarser than IASI's 0.25 cm^{-1} and finer than CrIS' 2.5 cm^{-1}, it is unable to capture the fine absorption lines like IASI, but shows more details than CrIS. The spectrally averaged differences between CIRAS and IASI/CrIS, or the bias, is almost zero. Plus, the STD between CIRAS and CrIS is slightly larger because of CrIS' coarser spectral resolution. Note that, because of the gap between the CrIS midwave and shortwave IR bands, CIRAS has a better spectral coverage on the shortwave side of the water band.

For conventional radiosonde observations of the main prognostic variables (temperature (K), specific humidity (kg kg^{-1}), and eastward and northward wind components (m s^{-1}), or $T/Q/U/V$, the HRNR is interpolated in time and space to the radiosonde times and locations observed in reality for each variable. This is somewhat unrealistic since the radiosonde drifts with the winds in reality and not with the winds in the HRNR. However, the overall distribution of radiosonde observations is reasonable. Simulated radiosonde errors are added using the eigenvector method (Jin et al. 2008; Li et al. 2008, 2009, 2018). These explicitly added errors have variances larger than actual radiosonde errors to account for representativeness errors (i.e. small scales present in reality but not in the nature run).
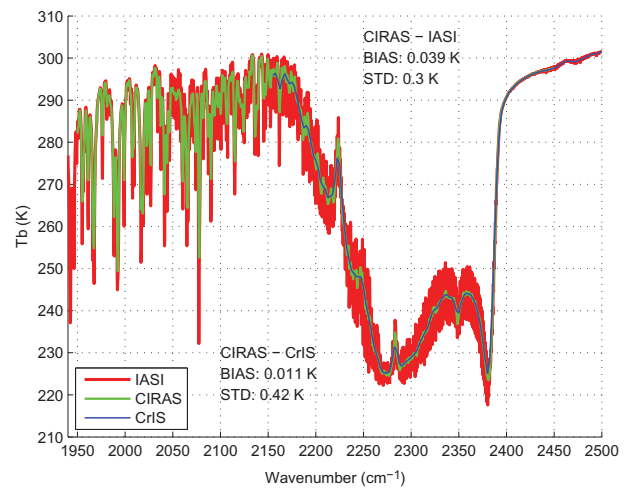
Figure 4. Comparison of simulated CIRAS T_b with IASI and CrIS for a randomly selected cloud-free profile, with statistics of bias and STD. The IASI/CrIS radiances are convolved with the CIRAS spectral response function before comparing with CIRAS radiances.

Figure 3. Density scatterplots (50 pixels on both the x- and y-axis) of simulated clear-sky T_b between ATMS and MicroMAS-2 for the 183.31 ± 1.0 GHz (left), 183.31 ± 3.0 GHz (middle), and 183.31 ± 7.0 GHz (right) channels, for 0000–1200 UTC 27 May 2006. The bias (ATMS minus MicroMAS-2), STD, correlation coefficient (R), and number of samples are also shown.

3. Assimilation

3.1. Assimilation strategy

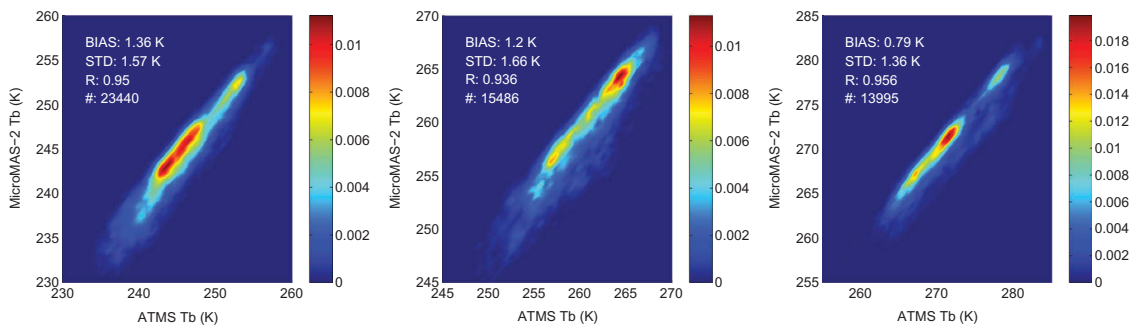All-sky radiance assimilation is now used operationally for MW observations and much progress has already been made for IR observations (Geer et al. 2018). Since these methods are not yet available and since there are some uncertainties in the calculation of cloudy radiance, as an approximation in this simulation study, we assimilate clear-sky soundings for IR and clear channel radiances for MW sounders. The community Gridpoint Statistical Interpolation (GSI) data assimilation system (v3.3) is used for this study. Since both MicroMAS-2 and CIRAS are future instruments, GSI cannot currently assimilate them. For the purpose of this study, both observations are converted to the observations that GSI is able to assimilate. The following strategy is used for MicroMAS-2. Linear regression relationships are constructed to use values of MicroMAS-2 T_b as predictors of ATMS T_b. ATMS has more channels (22) than MicroMAS-2 (12). Only 11 ATMS channels (7, 8, 9, 11, 12, 16, 18, 19, 20, 21, and 22) are well predicted. The regressions are then used to convert the MicroMAS-2 radiances simulated from the HRNR to ATMS channel radiances for the 11 well-predicted channels and these are converted to BUFR and assimilated directly by GSI. The GSI default quality control is used to remove radiances that are affected by clouds.

CIRAS observes radiances in the SWIR spectral region. Since no existing radiance observations in this spectral region are currently assimilated in the GSI system, there is no direct or indirect way to assimilate CIRAS radiances at this time. Instead, clear-sky 'sounding retrievals' of temperature and moisture profiles are used, following Jones, Koch, and Li (2017) and Li et al. (2018). The clear-sky sounding retrievals provide a decent spatial coverage of around 40%. For consistency, in this study, CrIS observations are assimilated in the form of sounding retrievals as well, although operational centers only assimilate CrIS radiances. Usually, CrIS retrievals are produced using a nonlinear physical one-dimensional variational retrieval method. Migliorini (2012) showed that the two assimilation approaches are theoretically equivalent. As pointed out in Li et al. (2018), assimilating sounding retrievals does have some advantages for hyperspectral IR sounders, such as using more channels and requiring less computational resource. However, the errors associated with sounding assimilation are not as easily defined as in radiance assimilation (Eyre et al. 1993). Both CIRAS and CrIS sounding retrievals are calculated using the same linear regression technique described by Li et al. (2018). The main difference is that CIRAS uses all 625 SWIR channels, while CrIS uses only the first 1146 longwave and midwave IR (LWIR and MWIR) channels.

Figure 5 shows the validation of the synthetic sounding retrievals of CIRAS and CrIS using HRNR as reference. Due to the coarse spectral resolution and narrow spectral coverage, CIRAS does not have the same sounding quality as CrIS. Besides, in reality, CIRAS channels around 4.3 µm are affected by NLTE, while the 1146 CrIS LWIR and MWIR channels are not affected by NLTE. As a result, real-world CIRAS sounding retrievals might not be as good as those shown in Figure 5. Both CIRAS and CrIS synthetic sounding retrievals are assimilated from the surface to 200 hPa in the GSI system. Note that there is no measurement covariance matrix in GSI for CrIS and CIRAS soundings. As is the case with radiosonde observations, vertical error correlations in CIRAS and CrIS sounding retrievals, which are due primarily to the retrieval algorithm, are only approximately accounted for in the assimilation by inflating the estimated observation error STDs.

3.2. Experiment design and evaluation strategy

OSSE can be used to study the value of new or proposed instruments as well as assimilation techniques (Atlas 1997; Atlas et al. 2015; Hoffman and Atlas 2016; Boukabara et al. 2016, 2018; Zhang et al. 2017; Cintineo et al. 2016; Otkin et al. 2011). Figure 6 shows the flow chart of the quick OSSE. This experimental setup, making use of a single short forecast as a nature run, is termed a quick OSSE to differentiate it from the full OSSE setup (Hoffman and Atlas 2016). The left-hand side shows the generation of the HRNR from the global OSSE analysis, which was detailed in Li et al. (2018) and briefly described in section 2.2. The synthetic observations of radiosonde and satellite observations are simulated from the HRNR using the methods described in sections 2.3 and 3.1. In this study, WRF-ARW v3.6.1 is used for assimilation and forecasting. Compared with WRF-NMM used for HRNR generation, the WRF-ARW used in the data assimilation and forecast experiments has a much coarser spatial resolution (9 km), reduced coverage (450 × 280 grid points; see Figure 2(a) for experiment coverage), and different parameterization schemes, including Thompson's new microphysics (Thompson et al. 2008), RRTMG longwave radiation, RRTMG shortwave radiation, Yonsei University planetary boundary layer, and Kain–Fritsch cumulus parameterizations. These model differences avoid the so-called identical twin problem for OSSEs, in which an identical model for nature run creation and for assimilation and forecasting results is used in unrealistically good analyses and forecasts due to the absence of model error.
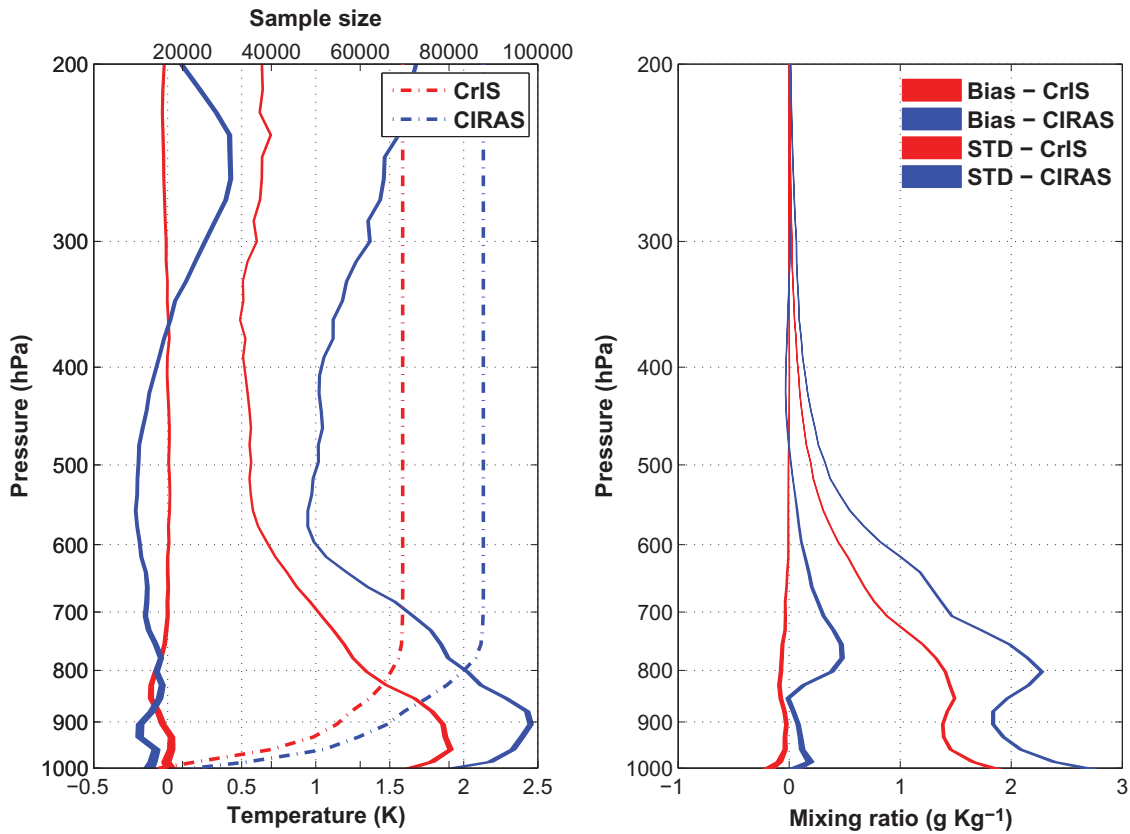
Figure 5. The STD (solid lines) and bias (semitransparent lines) of the atmospheric sounding retrievals of temperature (left) and mixing ratio (right) for CIRAS and CrIS in clear-sky only. The widths of the lines represent the 95% confidence interval. The dashed lines represent the sample size of each level.
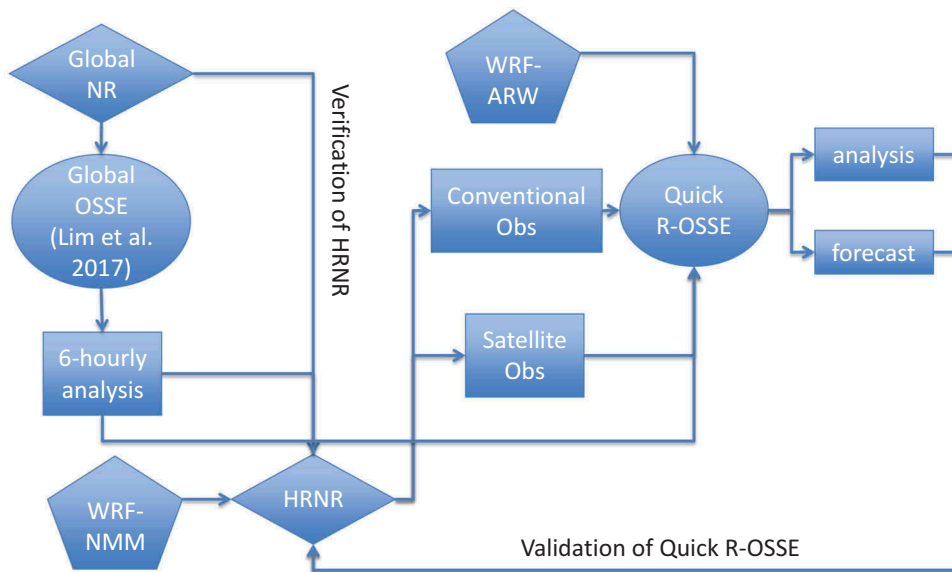
Figure 6. Flow chart of the quick R-OSSE.

The North American Mesoscale Forecast System background error covariance matrix (Wu 2005) is used as the background error covariance, and the variational bias correction method is used to update the satellite angle and mass bias for each cycle (Kleist et al. 2009). As with the HRNR, the six-hourly analyses from the global OSSE (Lim et al. 2017) are used as initial and boundary conditions. The experiments start at 0600 UTC 26 May.

Table 3. Observations used in each experiment. There is an MW and IR version of each CNTL, MO1, and MO2 experiment. CubeSat stands for MicroMAS-2 or CIRAS. The baseline observations include conventional RAOB, AMSU-A, and IASI from MetOp-B.

Name	Baseline observations	ATMS or CRIS	CubeSat @ 1330	CubeSat @ 1030 and 1630
GAP	✓			
CNTL	✓	✓		
MO1	✓		✓	
MO2	✓		✓	✓

After 6 h of spin-up, three cycles of assimilation are carried out every 6 h until 0000 UTC 27 May, followed by 18 h of forecast. The results are compared with the HRNR to evaluate the analysis and the forecast.

For this quick OSSE, not all existing observations are simulated/assimilated. Aircraft and surface observations, cloud track winds, and scatterometer winds, are not included in these experiments. Also, observations of satellite radiances are limited. All experiments include the conventional radiosonde observation (RAOB), AMSU-A and IASI from MetOp-B (the only morning orbit satellite that is not beyond its lifetime) as a baseline of the existing capability. For each instrument type (MW or IR), four experiments (summarized in Table 3) are conducted:

(a) GAP, which assumes both ATMS and CrIS on SNPP/JPSS are lost.
(b) The control run (CNTL), which includes either ATMS or CrIS to represent the existing capability.
(c) Mitigation option 1 (MO1), which replaces ATMS with MicroMAS-2 or CrIS with CIRAS in a 1330 orbit. This is the same orbit as SNPP/JPSS.
(d) Mitigation option 2 (MO2), which replaces ATMS with three MicroMAS-2 or CrIS instruments with three CIRAS instruments, with 1030, 1330, and 1630 orbits. The two additional satellites increase the data coverage of CubeSat.

This experimental design tests whether the addition of one or three MicroMAS-2 or CIRAS instruments is able to mitigate the loss of ATMS or CrIS.

3.3. Evaluation strategy

Following Li et al. (2018), one single value is calculated to represent the overall performance of the experiment based on the four important LSS parameters — one minus the equitable threat score for precipitation, convective available potential energy (CAPE), convective inhibition (CIN), and helicity — and the main prognostic variables ($T/Q/U/V$) at four standard atmospheric levels (250, 500, 700, and 850 hPa). For each parameter,

a normalized root-mean-square error (RMSE) is calculated. The normalization makes it possible to combine different parameters. Finally, a summary assessment metric (SAM) is calculated as a weighted average of the normalized RMSE values using the following weights: CAPE, 10%; CIN, 10%; helicity, 10%; rainfall, 20%; $T/Q/U/V$, 50%.

Because of the focus of this study on an LSS, the three LSS parameters (CAPE, CIN, and helicity) are given equal weight. Rainfall is given a heavier weight because rainfall includes both large-scale and convective rainfall. The SAM also averages over the last analysis time (0000 UTC 27 May) and the three forecast times (0600, 1200, and 1800 UTC 27 May). The SAM is calculated for each of the four experiments. Results are shown in section 4. Smaller SAM values (smaller weighted averages of normalized RMSEs) indicate better results.

4. Impact of micromas-2 and CIRAS on LSS analyses and forecasts

The left panel of Figure 7 shows the SAMs of the four MW experiments with a confidence interval of 95%. Comparing GAP with CNTL, ATMS is effective in reducing the SAM from 0.5028 to 0.4998 — a significant reduction of overall error by 0.6%. MO1 and MO2 are both able to reduce the SAM from the GAP scenario. However, a single MicroMAS-2 (MO1) in the 1330 orbit has a SAM of 0.5013 — still substantially larger than in CNTL. On the other hand, the MO2 experiment, with three MicroMAS-2 instruments, is more effective than MO1. The SAM of 0.4966 (a reduction of overall error by 1.2%) is significantly smaller than in CNTL. For this particular LSS case, a single MicroMAS-2 in ATMS orbit may reduce, but not eliminate, the gap caused by the loss of ATMS. A constellation of three MicroMAS-2 satellites in 1030, 1330, and 1630 orbits is able to mitigate the gap and make further improvements.

The right panel of Figure 7 shows a similar plot of SAMs for the four IR experiments. Again, comparing GAP with CNTL shows that CrIS is effective in reducing the SAM from 0.5054 to 0.4962 — a significant reduction of overall error by 1.8%. Plus, the two MOs are once again both able to reduce the SAM relative to the GAP scenario. A single CIRAS in the CrIS orbit reduces the SAM to 0.5003, but this is still significantly larger than the CNTL SAM. Three CIRAS instruments (MO2) are able to further reduce the SAM RMSE to 0.4978 — a reduction of overall error by 1.5%, which is closer but still substantially larger than the CNTL SAM. These results indicate that the single CIRAS in CrIS orbit may only partially mitigate the gap caused by the loss of CrIS. Three CIRAS
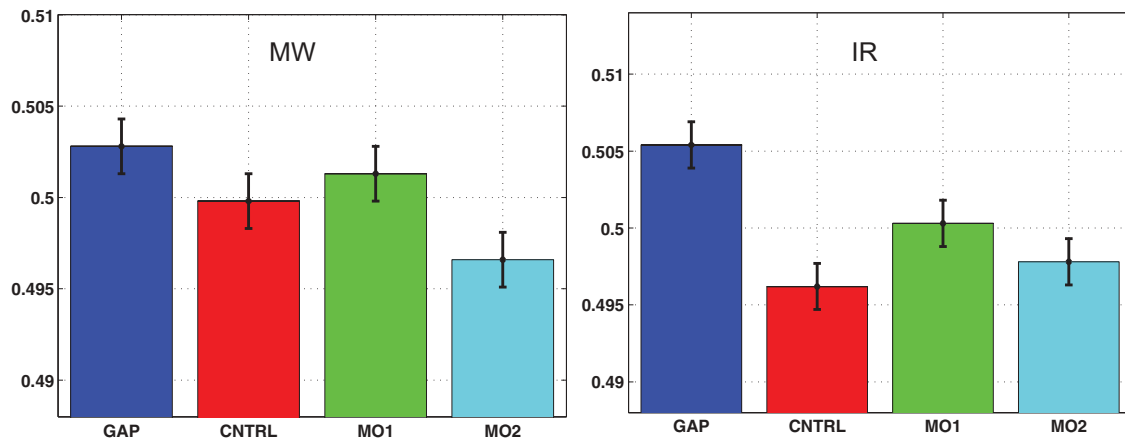
Figure 7. SAMs for the four (left) MW and (right) IR experiments. The 95% confidence intervals are plotted as small error bars at the ends of the color bars.

instruments with 1030, 1330, and 1630 orbits are better, but still do not eliminate the gap.

It appears that MicroMAS-2 is more capable of filling the gap than CIRAS. Recall that section 3.1 showed that MicroMAS-2 may predict 11 ATMS channels, which contain almost all the temperature and moisture sounding information between the model top (10 hPa) and surface from ATMS. Compared with channels used by Bormann, Fouilloux, and Bell (2013), the channels missing are those either peaking near the surface (such as channel 6) or around/above the model top (such as channels 13–15). Those missing channels would provide little useful information that can be assimilated in this study. CIRAS, on the other hand, due to coarser vertical resolution, contains much less sounding information, as shown in Figure 5, which makes it less capable of filling the gap.

It is important to point out that the SAM values presented in Figure 7 are sensitive to the weights used to average (see section 3.3 for more details). So, choosing different weights may change the overall error reduction percentage, but the main conclusions stand for the particular case in this study. This is because, for both type of instrument, the improvements are seen in most parameters. For example, if all eight of the parameters are given equal weight of 12.5%, the reductions of overall error by CNTRL, MO1, and MO2 from GAP are 0.48%, 0.39%, and 1.24% for MicroMAS-2, instead of 0.60%, 0.30%, and 1.23%. These values still support the conclusion that the constellation of three MicroMAS-2 satellites is more effective in mitigating the gap caused by the loss of ATMS than a single MicroMAS-2 instrument.

5. Summary and discussion

A quick R-OSSE has been conducted to investigate the value of CubeSat-based advanced MW and IR sounders on

LSS forecasts. Compared with traditional advanced sounders, CubeSat-based sounders are more cost-efficient to build and launch. As an example of potential cost savings, commercial launch costs, a major component of total mission costs, for CubeSat are an order of magnitude smaller than for traditional satellites (e.g. http://spaceflight.com/schedule-pricing/). However, CubeSats typically provide less information (i.e. fewer channels) over shorter lifetimes. Multiple units can be launched to improve the spatial and temporal coverage. The purpose of this study was to examine whether CubeSat-based advanced MW or IR sounders can be used to mitigate the loss of a conventional advanced MW or IR sounder, such as ATMS or CrIS on SNPP or JPSS. Our OSSE study of one particular LSS case indicated that: (1) a single MicroMAS-2 or CIRAS instrument has a positive impact on the LSS forecast; (2) more CubeSats with increased data coverage yield larger positive impacts. Therefore, both MicroMAS-2 and CIRAS have the potential to mitigate the loss of ATMS and CrIS on SNPP and JPSS, especially when there are multiple CubeSats in different orbits.

It is important to note the limitations of this study. The results presented were obtained through a quick OSSE, meaning the OSSE system was not calibrated and a single case was used. In the GAP scenario, only RAOB and MetOp-B observations were included to represent the existing baseline capability. Since SNPP was excluded from the GAP scenario, this represents an underestimation of the existing capability. However, comparisons to GAP highlight the impact of the sensors under study. Only clear-sky soundings and clear channel radiances were assimilated. This might have changed the relative value of IR compared to MW radiances. However, rapid progress is now being made in the use of all-sky radiances, mitigating this limitation. Note that AMVs can be obtained from IR and MW radiances but were not included in this study.

Also, for CIRAS, the CRTM coefficients do not have the NLTE effects included. However, this might be mitigated by improving the radiative transfer model (Chen et al. 2013; Matricardi, López-Puertas, and Funke 2018) and/or through the variational bias correction process. Furthermore, we ignored the issue of sensor calibration, which is expected to be a challenge for multiple advanced sounders onboard CubeSats (Weng 2017). These limitations are acceptable since this OSSE was an attempt to gauge the relative values of these sensors, and not their absolute value in current data assimilation and forecast systems. In this sense, this study provides an efficient methodology to study the value of future planned observing systems, such as the relatively inexpensive CubeSat-based sounding systems studied here. Finally, it should be noted that traditional satellite-based sounding systems are still extremely valuable for nowcasting, analysis, and forecasting, especially the advanced IR sounding system onboard geostationary satellites (Schmit et al. 2009).

Acknowledgments

Disclosure statement

Funding

ORCID

Zhenglong LI http://orcid.org/0000-0003-1737-735X
Robert ATLAS http://orcid.org/0000-0002-0706-3560

References

Atlas, R. 1997. "Atmospheric Observations and Experiments to Assess Their Usefulness in Data Assimilation (GtspecialIssueItData Assimilation in Meteology and Oceanography: Theory and Practice)." *Journal of the Meteorological Society of Japan* 75: 111–130. doi:10.2151/jmsj1965.75.1B_111.

Atlas, R., L. Bucci, B. Annane, R. N. Hoffman, and S. Murillo. 2015. "Observing System Simulation Experiments to Assess the Potential Impact of New Observing Systems on Hurricane Forecasting." *Marine Technology Society Journal* 49: 140–148. doi:10.4031/MTSJ.49.6.3.

Blackwell, W. J., S. Braun, R. Bennartz, C. Velden, M. DeMaria, R. Atlas, J. Dunion, et al. 2018. "An Overview of the TROPICS NASA Earth Venture Mission." *Quarterly Journal of the Royal Meteorological Society* (Accepted Author Manuscript). doi:10.1002/qj.3290.

Bormann, N., A. Fouilloux, and W. Bell. 2013. "Evaluation and Assimilation of ATMS Data in the ECMWF System." *Journal of Geophysical Research: Atmospheres* 118: 12970–12980. doi:10.1002/2013JD020325.

Boukabara, S., K. Ide, N. Shahroudi, Y. Zhou, T. Zhu, R. Li, L. Cucurull, R. Atlas, S. P. Casey, and R. N. Hoffman. 2018. "Community Global Observing System Simulation Experiment (OSSE) Package (CGOP): Perfect Observations Simulation Validation." *Journal of Atmospheric and Oceanic Technology* 35: 207–226. doi:10.1175/JTECH-D-17-0077.1.

Boukabara, S., I. Moradi, R. Atlas, S. P. F. Casey, L. Cucurull, R. N. Hoffman, K. Ide, et al. 2016. "Community Global OSSE Package (CGOP): Description and Usage." *Journal of Atmospheric and Oceanic Technology* 33: 1759–1777. doi:10.1175/JTECHD-16-0012.1.

Chen, Y., Y. Han, P. van Delst, and F. Weng. 2013. "Assessment of Shortwave Infrared Sea Surface Reflection and Nonlocal Thermodynamic Equilibrium Effects in the Community Radiative Transfer Model Using IASI Data." *Journal of Atmospheric and Oceanic Technology* 30: 2152–2160. doi:10.1175/JTECH-D-12-00267.1.

Chen, Y., Y. Han, P. Van Delst, and F. Z. Weng. 2010. "On Water Vapor Jacobian in Fast Radiative Transfer Model." *Journal of Geophysical Research* 115. doi:10.1029/2009JD013379.

Chen, Y., Y. Han, and F. Z. Weng. 2012. "Comparison of Two Transmittance Algorithms in the Community Radiative Transfer Model: Application to AVHRR." *Journal of Geophysical Research* 117. doi:10.1029/2011JD016656.

Cintineo, R. M., J. A. Otkin, T. A. Jones, S. Koch, and D. J. Stensrud. 2016. "Assimilation of Synthetic GOES-R ABI Infrared Brightness Temperatures and WSR-88D Radar Observations in a High-Resolution OSSE." *Monthly Weather Review* 144 (9): 3159–3180. doi:10.1175/MWR-D-15-0366.1.

Eyre, J. R., G. A. Kelly, A. P. McNally, E. Andersson, and A. Persson. 1993. "Assimilation of TOVS Radiance Information through One-Dimensional Variational Analysis." *Quarterly Journal of the Royal Meteorological Society* 119: 1427–1463. doi:10.1002/qj.49711951411.

Geer, A. J., K. Lonitz, P. Weston, M. Kazumori, K. O. Y. Zhu, E. H. Liu, A. Collard, et al. 2018. "All-Sky Satellite Data Assimilation at Operational Weather Forecasting Centres." *Quarterly Journal of the Royal Meteorological Society* 144: 1191–1217. doi:10.1002/qj.3202.

Hoffman, R. N., and R. Atlas. 2016. "Future Observing System Simulation Experiments." *Bulletin of the American Meteorological Society* 97: 1601–1616. doi:10.1175/BAMS-D-15-00200.1.

Jin, X., J. Li, T. J. Schmit, J. L. Li, M. D. Goldberg, and J. J. Gurka. 2008. "Retrieving Clear-Sky Atmospheric Parameters from SEVIRI and ABI Infrared Radiances." *Journal of Geophysical Research* 113: D15310. doi:10.1029/2008JD010040.

Jones, T. A., S. E. Koch, and Z. Li. 2017. "Assimilating Synthetic Hyperspectral Sounder Temperature and Humidity Retrievals to Improve Severe Weather Forecasts." *Atmospheric Research* 186: 9–25. doi:10.1016/j.atmosres.2016.11.004.

Kleist, D. T., D. F. Parrish, J. C. Derber, R. Treadon, W. Wu, and S. Lord. 2009. "Introduction of the GSI into the NCEP Global Data Assimilation System." *Weather and Forecasting* 24: 1691–1705. doi:10.1175/2009WAF2222201.1.

Li, J., J. Li, J. Otkin, T. J. Schmit, and C. Liu. 2011. "Warning Information in A Preconvection Environment from the Geostationary Advanced Infrared Sounding System - A Simulation Study Using IHOP Case." *Journal of Applied Meteorology and Climatology* 50: 776–783. doi:10.1175/2010JAMC2441.1.

Li, J., C.-Y. Liu, P. Zhang, and T. J. Schmit. 2012. "Applications of Full Spatial Resolution Space-Based Advanced Infrared Soundings in the Preconvection Environment." *Weather and Forecasting* 27: 515–524. doi:10.1175/WAF-D-10-05057.1.

Li, Z., J. Li, W. P. Menzel, T. J. Schmit, J. P. Nelson III, J. Daniels, and S. A. Ackerman. 2008. "GOES Sounding Improvement and Applications to Severe Storm Nowcasting, Geophys." *Research Letters* 35: L03806. doi:10.1029/2007GL032797.

Li, Z., J. Li, P. Wang, A. Lim, J. Li, T. J. Schmit, R. Atlas, S.-A. Boukabara, and R. Hoffman. 2018 Oct. "Value-Added Impact of Geostationary Hyperspectral Infrared Sounder on Local Severe Storm Forecasts – Via a Quick Regional OSSE." *Advances in Atmospheric Sciences* 35 (10): 1217–1230. doi:10.1007/s00376-018-8036-3.

Li, Z. L., J. Li, W. P. Menzel, J. P. Nelson III, T. J. Schmit, E. Weisz, and S. A. Ackerman. 2009. "Forecasting and Nowcasting Improvement in Cloudy Regions with High Temporal GOES Sounder Infrared Radiance Measurements." *Journal of Geophysical Research* 114: D09216. doi:10.1029/2008JD010596.

Lim, A., Z. Li, J. A. Jung, A. Huang, J. Woollen, F. W. Nagle, G. Quinn, et al. 2017. "Impact Analysis of LEO Hyperspectral Sensor Ifov Size on the Next Generation High-Resolution NWP Model Forecast Performance." Conference on Integrated Observing and Assimilation Systems for the Atmosphere, Oceans, and Land Surface, 21st, Seattle, WA, 21–26 January 2017. Boston, MA: American Meteorological Society

Matricardi, M., M. López-Puertas, and B. Funke. 2018. "Modeling of Nonlocal Thermodynamic Equilibrium Effects in the Classical and Principal Component-Based Version of the RTTOV Fast Radiative Transfer Model." *Journal of Geophysical Research: Atmospheres* 123: 5741–5761. doi:10.1029/2018JD028657.

Menzel, W. P., T. J. Schmit, P. Zhang, and J. Li. 2018. "Satellite-Based Atmospheric Infrared Sounder Development and Applications." *Bulletin of the American Meteorological Society* 99: 583–603. doi:10.1175/BAMS-D-16-0293.1.

Migliorini, S. 2012. "On the Equivalence between Radiance and Retrieval Assimilation." *Monthly Weather Review* 140: 258–265. doi:10.1175/MWR-D-10-05047.1.

Otkin, J. A., D. C. Hartung, D. D. Turner, R. A. Petersen, W. F. Feltz, and E. Janzon. 2011. "Assimilation of Surface-Based Boundary Layer Profiler Observations during a Cool-Season Weather Event Using an Observing System Simulation Experiment. Part I: Analysis Impact." *Monthly Weather Review* 139 (8): 2309–2326. doi:10.1175/2011MWR3622.1.

Pagano, T. S., C. Abesamis, A. Andrade, H. Aumann, S. Gunapala, C. Heneghan, R. Jarnot, et al. 2017. "Design and Development of the CubeSat Infrared Atmospheric Sounder (CIRAS), Proc. SPIE 10402." *Earth Observing Systems* XXII (September 5): 1040209. doi:10.1117/12.2272839.

Schmit, T. J., J. Li, S. A. Ackerman, and J. J. Gurka. 2009. "High Spectral and High Temporal Resolution Infrared Measurements from Geostationary Orbit." *Journal of Atmospheric and Oceanic Technology* 26: 2273–2292. doi:10.1175/2009JTECHA1248.1.

Thompson, G., P. R. Field, R. M. Rasmussen, and W. D. Hall. 2008. "Explicit Forecasts of Winter Precipitation Using an Improved Bulk Microphysics Scheme. Part II: Implementation of a New Snow Parameterization." *Monthly Weather Review* 136: 5095–5115. doi:10.1175/2008MWR2387.1.

Weng, F. 2017. "Challenges of Using Small Satellite Data in Numerical Weather Prediction Models." Seventh Conference on Transition of Research to Operations, Paper J11.5, 23–26 January, Seattle Washington: AMS. Recorded presentation available online at https://ams.confex.com/ams/97Annual/webprogram/Paper310116.html

Wu, W.-S. 2005. "Background Error for NCEP's GSI Analysis in Regional Mode." 4th WMO International Symposium on Assimilation of Observations in Meteorology and Oceanography, 18–22 April 2005. Prague, Czech Republic.

Yang, J., Z. Zhang, C. Wei, L. Feng, and Q. Guo. 2017. "Introducing the New Generation of Chinese Geostationary Weather Satellites, Fengyun-4." *Bulletin of the American Meteorological Society* 98: 1637–1658. doi:10.1175/BAMS-D-16-0065.1.

Zhang, S., Z. Pu, D. J. Posselt, and R. Atlas. 2017. "Impact of CYGNSS Ocean Surface Wind Speeds on Numerical Simulations of a Hurricane in Observing System Simulation Experiments." *Journal of Atmospheric and Oceanic Technology* 34: 375–383. doi:10.1175/JTECH-D-16-0144.1.